Calculation of delayed-neutron energy spectra in a quasiparticle random-phase approximation–Hauser-Feshbach model

T. Kawano,* P. Möller, and W. B. Wilson
Theoretical Division, Los Alamos National Laboratory, Los Alamos, New Mexico 87545, USA
(Received 2 July 2008; published 6 November 2008)

Theoretical β-delayed-neutron spectra are calculated based on the Quasiparticle Random-Phase Approximation (QRPA) and the Hauser-Feshbach statistical model. Neutron emissions from an excited daughter nucleus after β decay to the granddaughter residual are more accurately calculated than in previous evaluations, including all the microscopic nuclear structure information, such as a Gamow-Teller strength distribution and discrete states in the granddaughter. The calculated delayed-neutron spectra agree reasonably well with those evaluations in the ENDF decay library, which are based on experimental data. The model was adopted to generate the delayed-neutron spectra for all 271 precursors.

DOI: 10.1103/PhysRevC.78.054601 PACS number(s): 24.10.−i, 23.40.−s

I. INTRODUCTION

Realistic descriptions of β-delayed neutrons are particularly important in contexts that involve the nuclear fission process. Fission fragments shed their considerable excitation energies by emitting several prompt γ rays and neutrons before reaching the ground states of the precursors. These fission products are neutron-rich and therefore β^- decay toward stability. When the final-state energy of a β-decay daughter is higher than the neutron separation energy S_n, emission of delayed neutrons is energetically possible. The prompt and delayed neutrons can be distinguished from each other because of the different timescales of the two processes, about 10^{-16} and 10^{-2} s to 10 s, respectively. The specifics of the β-delayed-neutron spectra can be used to identify the fissioning configuration, because the precursor yields depend on the fissioning systems.

Because many different nuclei are produced in fission, a detailed knowledge of the properties of each of the individual precursors and their yields is required to fully characterize the delayed neutrons. Macroscopic observables, such as total delayed-neutron yields, six-group constants, and aggregate energy spectra, can be derived from the properties of the delayed-neutron emission from each individual precursor [1–3]. Such a microscopic treatment of the delayed-neutron emission from the individual fission products requires a large-scale nuclear-structure database and theoretical models for neutron emission probabilities.

Theoretical calculations of delayed-neutron spectra have been performed earlier [4–8]. In these studies simple models were invoked for the β-strength function and the neutron emission probabilities from daughter nuclei, including the competition with γ-ray emission. However, the reproduction of the experimental delayed-neutron spectra is not satisfactory. Here we introduce more recent and much more microscopic models of the β-strength functions that have been well benchmarked with respect to experimental data for integral properties such as β-decay half-lives and delayed-neutron emission probabilities [9–11].

In this study, we have developed a more microscopic model to calculate the energy spectrum based on a combination of microscopic nuclear-structure models and statistical nuclear-reaction theories. Brady [2] identified the 271 most important precursors that can emit delayed neutrons. We calculate microscopically the β-decay probabilities from the precursors to all accessible states in the daughter nuclei in a Quasiparticle Random-Phase Approximation (QRPA) [9,10]. The final states in the daughter nuclei again decay by emitting a neutron or γ rays. The branching ratios are calculated in the Hauser-Feshbach statistical model. A microscopic theory for the delayed-neutron emission is especially needed when the fissioning systems are minor actinides, such as Am and Cm, because their fission-product yields are different from U and Pu and the aggregate delayed-neutron data are often unavailable. Future applications of our work here are to extend our approach to astrophysical studies [12]. This will require additional model extensions because many studies, for example, those involving reactions in the neutron star crusts, occur in very extreme environments. Such nucleosynthesis network calculations ideally would involve thousands of neutron- and proton-rich, unstable nuclei. These networks are populated by β decay, electron capture, and neutron and proton emission, all of which can be studied in our approach.

II. THEORETICAL MODELS

A. QRPA for β decay

The calculation of delayed-neutron energy spectra is divided into two stages: (1) the β decay of the precursor (Z, A) and (2) the statistical decay of the daughter nucleus $(Z+1, A)$ to the granddaughter $(Z+1, A-1)$, where Z is the atomic number and A is the mass number of precursor. The delayed-neutron emission process is shown schematically in Fig. 1.

Historically many studies assumed that intrinsic nuclear structure is not important. The β-strength function S_β for a

*kawano@lanl.gov

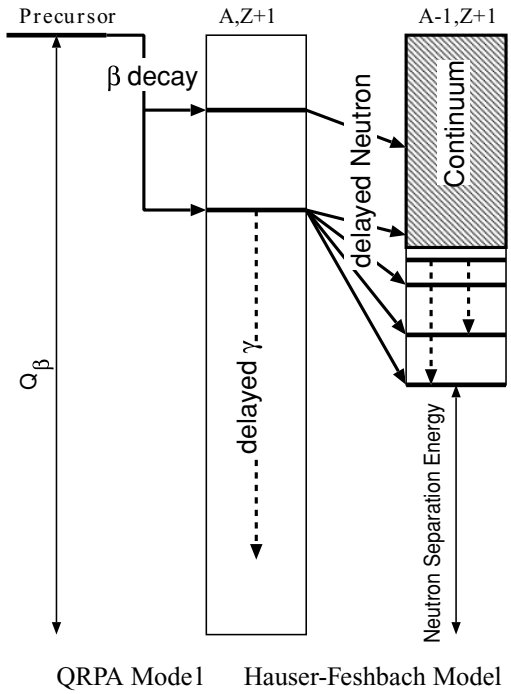

FIG. 1. Relative energies for the β-delayed neutron emission are shown schematically. The left-hand side shows that the precursor β-decays to a $(A, Z+1)$ nucleus with the maximum electron energy of Q_β, and the right-hand side describes the delayed-neutron emission part. Delayed-γ emission is also possible, which is indicated by dotted arrows.

transition to a state in the daughter nucleus at the excitation energy E_x was assumed to be given by [4]

$$S_\beta(E_x) = \sum \rho(E_x, J^\pi)|M|^2 D^{-1}, \tag{1}$$

where $\rho(E_x, J^\pi)$ is the level density of daughter with spin J and parity π at excitation energy E_x, $|M|^2$ is the average β-transition probability to the final state, D is the vector coupling constant ($\sim$6250 s), and the sum runs over J^π. It was assumed that the matrix element $|M|^2$ is energy-independent, and hence the β-strength function is proportional to the level density.

The delayed-neutron spectra were calculated from Eq. (1) by multiplying with the neutron decay probability to the final granddaughter state. The level structure of the granddaughter nucleus was not taken into account; therefore the calculated spectra were "structureless," which contradicts experimental delayed-neutron spectra, which often reveal complicated structure [4].

The various decay steps considered in our model are basically the same as those in the studies in the past; however, all quantities are now treated within a more microscopic framework. The Q_β values are calculated from the Finite Range Droplet Model (FRDM) masses [13], and the decay matrix elements $\langle f|\beta_{\rm GT}|i\rangle$ from the QRPA model [9,10]. More limited and less global QRPA models of delayed-neutron emission have been studied previously, see, for example, Delion, Santos, and Schuck [15] and Borzov [16].

The starting point for our model for calculating the β-decay rates from precursor to daughter is solving the Schrödinger Equation for the nuclear wave function and single-particle energies in a deformed single-particle potential with additional residual interactions (pairing and Gamow-Teller interactions). The model is extensively discussed and compared to β-decay data in Refs. [9–11]. Because the transition energies and rates for β decay depend on the specific level structure in the daughter nucleus it is essential to calculate these level structures as accurately as possible. The level structure depends crucially on the deformation of the nuclei. We obtain the nuclear deformation parameters (ε_2, ε_4, and ε_6) for nuclei across the nuclear chart from our calculation of ground-state masses and deformations [13]. The results on nuclear masses and deformations compare extremely well with experimental data and the model also has impressive predictive capability (see Refs. [13,14] and references therein).

This model allows us to calculate the β-decay rate for nuclei across the entire nuclear chart. It provides the branching ratios $b^{(k)}$ from the initial parent state to the various daughter states $E^{(k)}$, where k is the index of kth excited state in the daughter nucleus. The decay-rate distribution is smoothed by a Gaussian with the width Γ of 30 or 100 keV [17], which were estimated empirically by considering experimental energy resolution and single-particle energy spreading. The smoothed decay-rate distribution in the daughter nucleus $\omega(E_x)$ is

$$\omega(E_x) = c \sum_k b^{(k)} \frac{1}{\sqrt{2\pi}\Gamma} \exp\left\{-\frac{[E^{(k)} - E_x]^2}{2\Gamma^2}\right\}, \tag{2}$$

where E_x is the excitation energy of the daughter nucleus and c is the normalization constant given by the condition

$$\int_{Q_\beta - S_{\rm n}}^{Q_\beta} \omega(E_x) dE_x = 1, \tag{3}$$

where $S_{\rm n}$ is the neutron separation energy.

Figure 2 shows an example of the Gamow-Teller decay-rate distribution for ^{146}Xe, which β-decays to the delayed-neutron emitter ^{146}Ce. The dotted vertical lines are the calculated

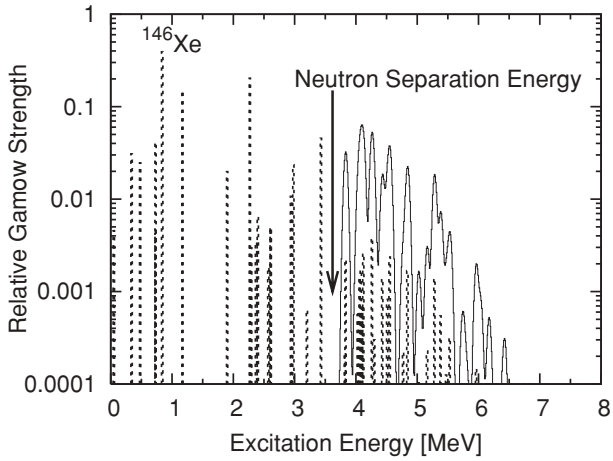

FIG. 2. Relative Gamow-Teller decay-probability distribution for β decay of ^{146}Xe calculated by the QRPA model (dotted lines) and the Gaussian-broadened distribution (solid line). The Gaussian-broadened distribution in the energy window above $S_{\rm n}$ is renormalized according to Eqs. (2) and (3).

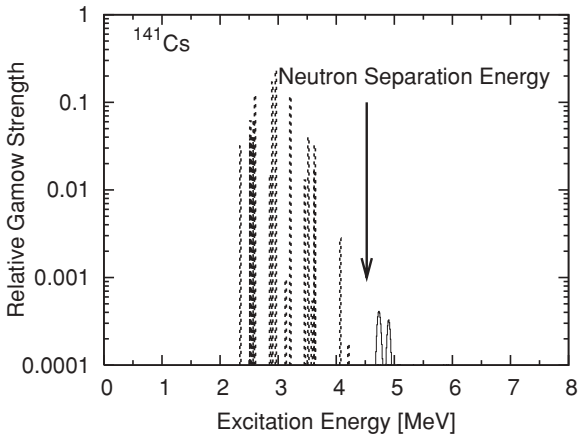

FIG. 3. Relative Gamow-Teller decay-probability distribution for β decay of ^{141}Cs calculated by the QRPA model (dotted lines) and the Gaussian-broadened distribution (solid line). See also the caption of Fig. 2.

relative distribution of the decay probabilities by the QRPA model, and the solid curve is the Gaussian-broadened distribution in Eqs. (2) and (3). The neutron emission originates in the excitation-energy interval from S_n to Q_β. This defines minimum and maximum delayed-neutron energies.

The Gamow-Teller decay rate for ^{141}Cs is shown in Fig. 3. In this case, only a few quasiparticle states with $E_x > S_n$ are found, and the delayed-neutron emission probability from ^{141}Ba* is therefore quite small, only 0.029% [30].

B. Neutron emission from excited states

The statistical theory has been applied to calculate the decay probabilities of the excited states in the past [4–8]. However, due to the lack of detailed nuclear-structure calculations and approximations made for the neutron and γ-ray penetration probabilities, these studies only reproduce the general trend of the experimental data.

In this study, we model the delayed-neutron emission process in a more microscopic fashion. The neutron emission from the daughter nucleus after β decay is calculated with the statistical Hauser-Feshbach theory [18]. We assume that the excited states in the daughter nucleus are compound states. This assumption is fulfilled in our case, because when the excitation energy is high enough then the initial quasiparticle state promptly reaches a thermoequilibrium state.

The excited state in the daughter nucleus following the β decay, labeled by (E_x, J^π), where E_x is the excitation energy given by the QRPA calculation in Eq. (2) and J^π is the spin and parity of the state, decays by emitting either γ rays or a delayed neutron. The spin and parity selection rules between the precursor and the daughter nucleus are followed. The γ-ray emission affects the neutron spectrum at low emission energies only, and the dominant process is still the neutron emission.

For the neutron emission from (E_x, J^π) to $(E'_x, J^{\pi\prime})$ in the granddaughter nucleus, we calculate the neutron transmission coefficients $T_{lj}(\epsilon)$ by solving the Schrödinger equation for a given optical potential, where $\epsilon = E_x - E'_x - S_n$ is the emitted neutron energy and l and j are the orbital angular momentum and the spin of the emitted neutron. Because we deal with neutron-rich unstable nuclei, we employ the Koning-Delaroche global optical potential [19] that has an isospin dependent term.

The excited state in the granddaughter can be a discrete level with fixed J^π, or it can be in the continuum. We include all the discrete level information from the Reference Input Parameter Library, RIPL-2 [20]. Above the maximum excitation energy for which J^π of the level is known, the Gilbert-Cameron level density formula [21] is used, which is a hybrid formulation incorporating the constant-temperature model and the Fermi-gas model. The parameters in the level density formula are taken from phenomenological systematics [22], which involve an extrapolation of the level density parameters from the valley of stability toward neutron-rich unstable nuclei.

The γ-ray competition is included in the Hauser-Feshbach calculations. The γ-ray transmission coefficients are generated with the generalized Lorentzian $E1$ strength function [23], and the Giant Dipole Resonance parameters are taken from RIPL-2. We also include the $M1$ and $E2$ transitions. Because experimental averaged γ widths $\langle\Gamma_\gamma\rangle$, which are usually given by a resonance analysis, are not available for the nuclei of interest to us, we adopt the simple systematics of $\langle\Gamma_\gamma\rangle = 2970A^{-2.08}$ eV, where A is the mass number. This systematics is obtained by a least-squares fit to the evaluated $\langle\Gamma_\gamma\rangle$ values in Ref. [20]. All the calculations are done with a modified version of the optical and Hauser-Feshbach models code CoH [24].

The Hauser-Feshbach calculation gives transition probabilities to the different final discrete states $p_d(\epsilon)$ and to the continuum state $p_c(\epsilon)$. The neutron emission spectrum from a fixed daughter excitation energy E_x is

$$\psi(E_x, \epsilon) \propto p_d(\epsilon) + p_c(\epsilon)\rho(E'_x)dE'_x, \tag{4}$$

where $\rho(E'_x)$ is the level density of the granddaughter nucleus. Here we omitted indexes of spin and parity, but all transitions satisfy the appropriate selection rules. Because the final delayed-neutron spectrum is normalized as below, the normalization constant in Eq. (4) is not necessary. The ground-state spin and parity I^π of precursors are usually known. However although we obey the selection rules in our calculations of allowed Gamow-Teller β-decay rates, the J^π of the daughter nucleus are not given. To obtain these we would need to introduce additional residual interactions coupling the excited quasiparticles in the daughter nucleus. We address our incomplete knowledge of the quantum numbers of the daughter state by calculating Eq. (4) for three cases, namely, $J = I, I \pm 1$ with the same parity, and averaging them.

With Eq. (2), the delayed-neutron energy spectrum $\phi(\epsilon)$ is calculated as

$$\phi(\epsilon) = d\int_{Q_\beta - S_n}^{Q_\beta} \omega(E_x)\psi(E_x, \epsilon)dE_x, \tag{5}$$

where d is the normalization constant to ensure

$$\int_0^\infty \phi(\epsilon)d\epsilon = 1. \tag{6}$$

III. RESULTS AND DISCUSSIONS

A. Structure in neutron spectra

Hauser-Feshbach calculations are performed for all excited states in the daughter nucleus in energy bins of 10 keV. We have generated delayed-neutron spectra for the 271 precursors in the ENDF/B-VI decay-data library. In this library, data for 36 nuclei out of 271 are based on experiments and can therefore be used to benchmark our model. Note that the more recent data library, ENDF/B-VII [25], contains more precursors of β-delayed neutron emission. However, the most important delayed-neutron emitting fission products are the same.

Figure 4 compares the calculated delayed-neutron spectra for ^{80}Ga and ^{146}Xe to the ENDF/B-VI data, with the choice $\Gamma = 30$ keV in Eq. (2). The ENDF/B-VI evaluation for ^{80}Ga is based on experimental data [26–28] in the energy range 100 keV–1.05 MeV, and the BETA code [8] was employed to extrapolate the spectrum outside the range [3]. Because our calculations consider all the possible transitions between the excited states in the daughter and granddaughter nuclei, the details of the complicated structure in the experimental spectra, which cannot be reproduced by an evaporation or Maxwellian spectrum [29], are present in our results. We emphasize that our calculations do not include any parameter-adjustment procedures to the spectra, but they represent theoretical results and predictions. In the case of ^{146}Xe [Fig. 4(b)] the ENDF/B-VI decay data library gives a simple evaporation spectrum because of the lack of experimental information. In contrast, our model predicts several peaks in the spectrum.

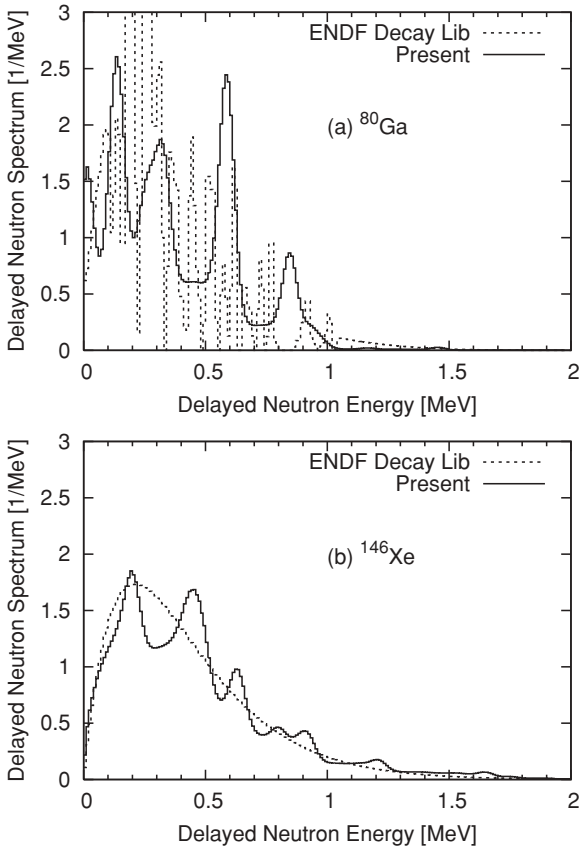

FIG. 4. Comparisons of calculated and evaluated delayed-neutron energy spectra for (a) ^{80}Ga and (b) ^{146}Xe. The dotted curves are the evaluated data in the ENDF decay library, and the solid curves are the QRPA and Hauser-Feshbach calculations.

The present calculation reproduces rather well the energy domain in which delayed neutrons are emitted. However, it does not reproduce the structure of the experimental spectrum perfectly. In the case of ^{80}Ga, the QRPA calculation gives the transition probabilities to all the states in ^{80}Ge, but only 1% of them decay to the states that can emit a delayed neutron. For example, the calculated result includes three strong transitions: 0.15% of the total β decay produces an excited ^{80}Ge state at 8.17 MeV, 0.26% decays to an 8.62 MeV excited state, and 0.14% decays to an 8.88 MeV excited state. On the other hand, the nuclear structure of ^{79}Ge is known to be 0.0 keV $(1/2)^-$, 0.186 keV$(7/2)^+$, 0.391 keV$(9/2)^+$, and so on [30]. Therefore the lowest peak of the neutron spectrum around 0.14 MeV in Fig. 4 corresponds to the neutron emission from the 8.17 MeV state in ^{80}Ge leaving ^{79}Ge at its ground state ($\epsilon = 8.17 - 8.03 = 0.14$ MeV, where 8.03 MeV is the neutron separation energy). The next strongest peak around 0.6 MeV corresponds to the 8.62 MeV state in ^{80}Ge to the ^{79}Ge ground state ($\epsilon = 8.62 - 8.03 = 0.59$ MeV), and so forth. Each peak of the neutron spectrum can be identified in such a way.

The peak locations in the delayed-neutron spectrum are sensitive to the predicted single-particle energies in the daughter nucleus. It is obvious that a 100 keV shift of the single-particle energy gives the same amount of peak shift in the neutron spectrum. The calculated excitation energies of the daughter nucleus are higher than the neutron separation energies, typically 5–8 MeV, and a 100 keV energy difference is only 2% or less. No current state-of-the-art nuclear structure model that can be applied to nuclei in this mass region can predict the excitation energies to such a high accuracy. However, despite these limits to the accuracy of our model, our benchmark studies are encouraging and show that the steps we have taken here lead to improved neutron spectra relative to the existing evaluations based on more simplistic models.

B. Cesium isotopes

We made additional comparisons for cesium isotopes with the data in the ENDF/B-VI decay library. The evaluations are based on the experimental data from the University of Mainz [31] and INEL [32], and an extrapolation was made with the BETA code [8]. In the case of ^{148}Cs, the evaluation was done purely by the BETA code calculation. The calculated delayed-neutron spectra for $^{141\text{-}148}$Cs are shown in Fig. 5. To see a gross structure of the energy spectra, we also adopted $\Gamma = 100$ keV in Eq. (2) for the Gamow-Teller decay rate broadening, which is shown by the thick curves in these plots. Generally agreements between the calculated results and experimental data (fluctuating part in the ENDF spectra) are fair, in both even and odd mass cases. It is apparent that the delayed-neutron spectrum cannot be fitted by a simple evaporation spectrum, and such an approximation may bring a large uncertainty in both the low-energy and high-energy regions.

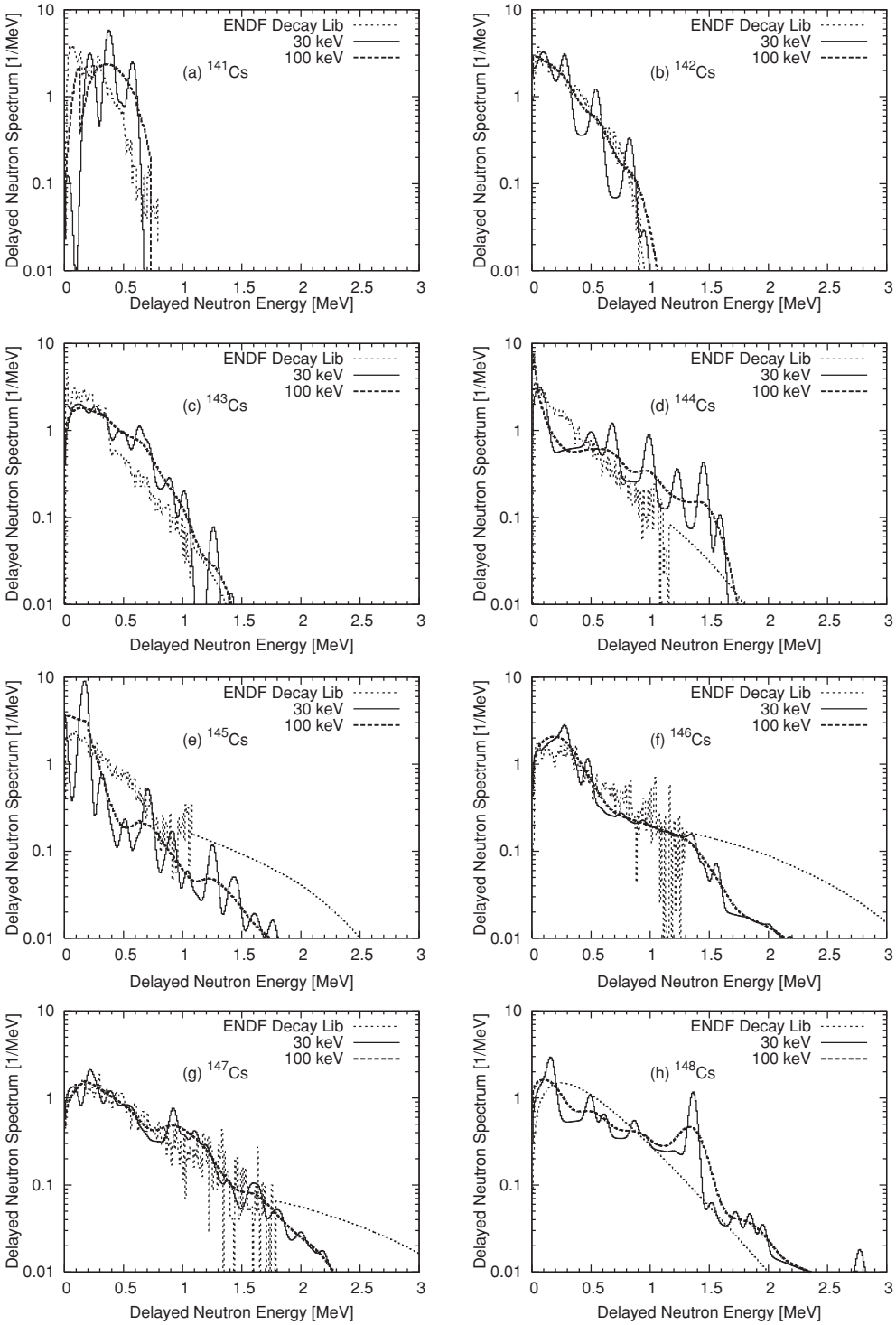

FIG. 5. Comparisons of calculated delayed-neutron energy spectra for $^{141-148}$Cs with the data in the ENDF decay library. The thick solid curves are the $\Gamma = 100$ keV case, and the thin curves are the $\Gamma = 30$ keV case.

For ^{141}Cs, the delayed-neutron emission takes place in a narrow energy window. The maximum neutron energy is defined by $E_{\max} = Q_\beta - S_n$, and our model calculates this energy window automatically. In the case of ^{141}Cs, $Q_\beta - S_n = 0.73$ MeV, which corresponds to the sharp cutoff of the neutron spectrum on the high-energy side.

C. Bromine isotopes

Figure 6 shows the calculated delayed-neutron spectra for bromine isotopes compared with the evaluated data in the ENDF decay library. The evaluations are based on the experimental data from Studsvik [27,28] for ^{88}Br and from Mainz [31] for the other isotopes. The extrapolation down to

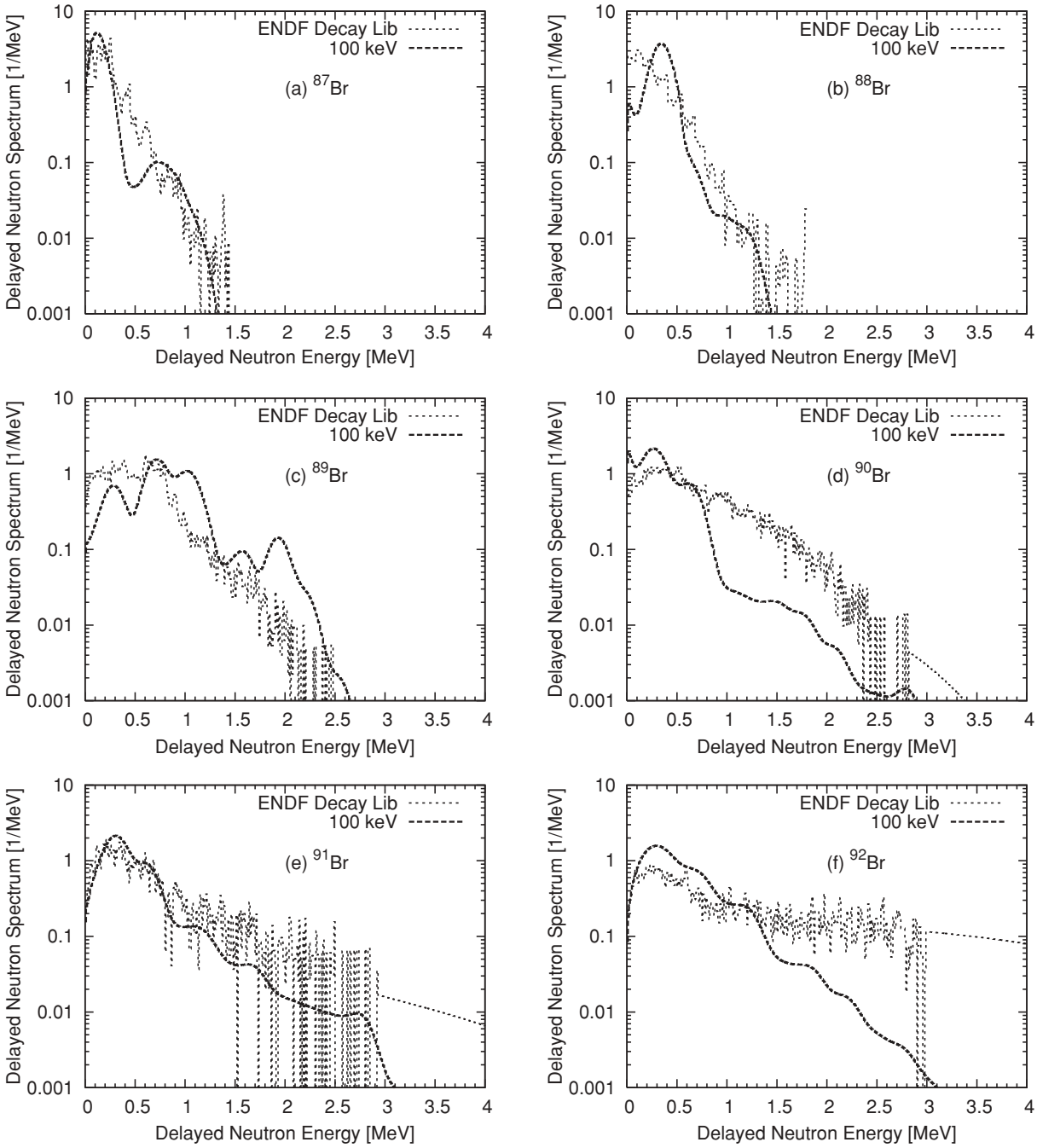

FIG. 6. Comparisons of calculated delayed-neutron energy spectra for $^{87-92}$Br with the data in the ENDF decay library. The Gaussian broadening width is taken to be $\Gamma = 100$ keV.

zero energy and up to $E_{\max}$ was done by the BETA code. In Fig. 6 only calculations for $\Gamma = 100$ keV are shown. Agreement with data, of similar quality as was obtained for the cesium cases, is obtained here; our model reproduces, although not perfectly, the overall gross structure of the experimental spectra.

For the ^{90}Br and ^{92}Br cases, the comparisons indicate we underestimate the higher energy component in the spectra. To quantify this observation we calculate average energies of the delayed-neutron spectra by

$$\bar{\epsilon} = \int_0^\infty \epsilon \phi(\epsilon) d\epsilon, \tag{7}$$

for both the experimental data (evaluations) and our calculated results. The results are shown in Fig. 7(a). The solid squares are $\bar{\epsilon}$ for the ENDF decay library, and the open circles are our results. In general the trends of our results are similar to those of ENDF, except for ^{92}Br. We see an unexpected jump

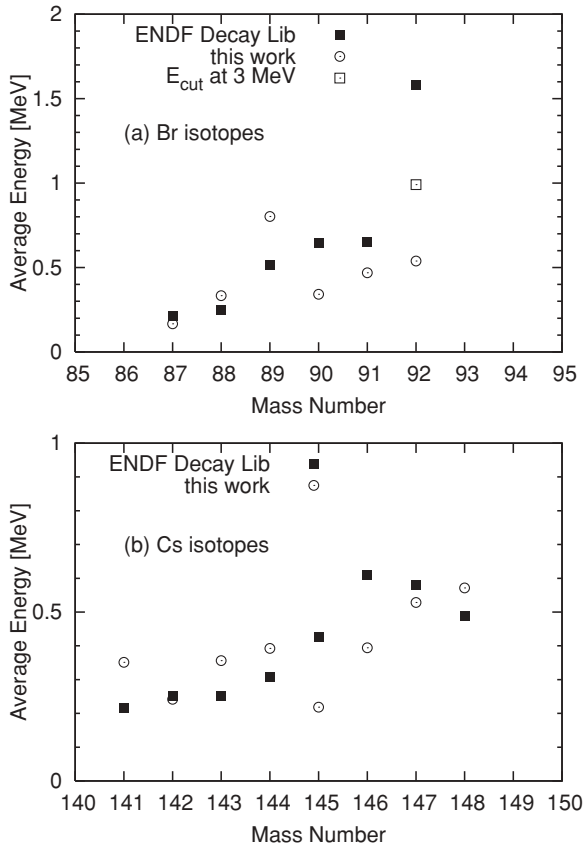

FIG. 7. Average energies of the delayed-neutron energy spectra for (a) Br and (b) Cs isotopes. The solid squares are for the ENDF decay library, the open circles are our calculated results, and the open square in the top panel is the ^{92}Br in ENDF but the maximum energy $E_{\rm cut}$ is set to 3 MeV.

of $\bar{\epsilon}$ at $A = 92$. As shown in Fig. 6, the spectrum for ^{92}Br includes a calculated part above 3 MeV, and this might drive up $\bar{\epsilon}$ to 1.6 MeV. When $\bar{\epsilon}$ is determined by the data up to $E_{\rm cut} =$ 3 MeV, which is shown by the open square, $\bar{\epsilon}$ behaves more reasonably.

Figure 7(b) shows a comparison of calculated and evaluated average energies for Cs isotopes. The average energies of our results for ^{145,146}Cs are lower than those of the ENDF data, for the same reason as for ^{92}Br. As shown in Fig. 5, a large part of the evaporation spectra above 1 MeV in the ENDF data contributes to the higher value of $\bar{\epsilon}$.

We have also performed comparisons for 36 precursors spanning nuclei from ^{79}Ga to ^{147}Cs, for which evaluations were based on experimental data, and found that the general trend of the quality of the agreement between calculations and evaluations is similar to that for Cs and Br isotopes in Figs. 5 and 6. The energy domain of the spectra for each isotope is well reproduced; however, the peak locations are often shifted by several hundreds of keV when $\Gamma = 30$ keV is adopted.

Our comparisons to known data encouraged us to apply the model to produce delayed-neutron spectra for all 271 precursors. We believe that the 36 evaluations in the decay library are of high quality because they are directly obtained from experimental results (only occasionally with questionable extrapolations given by the BETA code). A simple model spectrum is given for the rest of the 235 precursors. One example is shown in Fig. 4(b). We propose to replace these data by our microscopic calculations, which should have more realistic shapes. These spectra can be used to derive integral delayed-neutron observables for various fissioning systems. Because our treatment of particle emission is not limited to the β-delayed neutrons, the same technique can be applied to other nuclear decay processes such as proton emission, β-delayed γ-ray emission (this is already a part of our modeling), β-delayed fission, and so on.

IV. CONCLUSION

We developed a more microscopic technique to calculate the delayed-neutron energy spectra for fission products. This technique obtains the β-decay rates from the FRDM and QRPA models and the neutron and γ-ray emission probabilities from the statistical Hauser-Feshbach model. The calculated delayed-neutron spectra, which are purely theoretical predictions, reasonably agree with those evaluations that are based on experimental data. As examples, comparisons for ^{80}Ga, cesium, and bromine isotopes are shown in this article. The calculated average energies for the spectra tend to be similar to those for the data in ENDF decay library. We have made these comparisons for 36 evaluations for which experimental data are available. After these benchmarks of the model we employed it to generate delayed-neutron spectra for all 271 precursors.

ACKNOWLEDGMENTS

We thank G. W. McKinney and L. Waters of Los Alamos National Laboratory for encouraging this work. This work was carried out under the auspices of the National Nuclear Security Administration of the U.S. Department of Energy at Los Alamos National Laboratory under Contract DE-AC52-06NA25396.

[1] T. R. England, W. B. Wilson, R. E. Schenter, and F. M. Mann, Nucl. Sci. Eng. **85**, 139 (1983).
[2] M. C. Brady, *Evaluation and Application of Delayed Neutron Precursor Data*, LA-11534-T thesis, Los Alamos National Laboratory, 1989.
[3] M. C. Brady and T. R. England, Nucl. Sci. Eng. **103**, 129 (1989).
[4] A. C. Pappas and T. Sverdrup, Nucl. Phys. **A188**, 48 (1972).
[5] S. Shalev and G. Rudstam, Nucl. Phys. **A230**, 153 (1974).
[6] G. Rudstam and S. Shalev, Nucl. Phys. **A235**, 397 (1974).
[7] O. K. Gjøtterud, P. Hoff, and A. C. Pappas, Nucl. Phys. **A303**, 281 (1978).
[8] F. M. Mann, C. Dunn, and R. E. Schenter, Phys. Rev. C **25**, 524 (1982).

[9] J. Krumlinde and P. Möller, Nucl. Phys. **A417**, 419 (1984).
[10] P. Möller and J. Randrup, Nucl. Phys. **A514**, 1 (1990).
[11] P. Möller, J. R. Nix, and K.-L. Kratz, At. Data Nucl. Data Tables **66**, 131 (1997).
[12] S. S. Gupta, A. Heger, P. Möller, and T. Kawano, in *Proceedings International Conference on Compond-Nuclear Reactions and Related Topics, Tenaya Lodge, Yosemite National Park, Fish Camp, CA, USA, 22–26 October 2007*, edited by J. Escher, F. S. Dietrich, T. Kawano, and I. Thompson, AIP Conf. Proc. **1005**, 221 (2008).
[13] P. Möller, J. R. Nix, W. D. Myers, and W. J. Swiatecki, At. Data Nucl. Data Tables **59**, 185 (1995).
[14] P. Möller, R. Bengtsson, K.-L. Kratz, and H. Sagawa, "Large-Scale Calculations of Nuclear-Structure Data for Simulation Data Bases," in *Proc. Int. Conf. on Nuclear Data for Science and Technology, Nice, France, 22–27 Apr. 2007*, edited by O. Bersillon, F. Gunsing, E. Bauge, R. Jacqmin, and S. Leray (EDP Sciences, 2008), pp. 69–72.
[15] D. S. Delion, D. Santos, and P. Schuck, Phys. Lett. B **398**, 1 (1997).
[16] I. N. Borzov, Phys. Rev. C **71**, 065801 (2005).
[17] H. Ohm, M. Zendel, S. G. Prussin, W. Rudolph, A. Schröder, K.-L. Kratz, C. Ristori, J. A. Pinston, E. Monnand, F. Schussler, and J. P. Zirnheld, Z. Phys. A **296**, 23 (1980).
[18] W. Hauser and H. Feshbach, Phys. Rev. **87**, 366 (1952).
[19] A. Koning and J.-P. Delaroche, Nucl. Phys. **A713**, 231 (2003).
[20] Reference Input Parameter Library, RIPL-2, IAEA-TECDOC, International Atomic Energy Agency (2004).
[21] A. Gilbert and A. G. W. Cameron, Can. J. Phys. **43**, 1446 (1965).
[22] T. Kawano, S. Chiba, and H. Koura, J. Nucl. Sci. Technol. **43**, 1 (2006).
[23] J. Kopecky and M. Uhl, Phys. Rev. C **41**, 1941 (1990).
[24] T. Kawano, "The Hauser-Feshbach-Moldauer Statistical Model with the Coupled-Channels Theory" (unpublished); T. Kawano, S. Chiba, T. Maruyama, Y. Utsuno, H. Koura, and A. Seki, in *Proceedings of the 2003 Symposium on Nuclear Data, JAERI, Tokai, Japan, 27–28 November 2003*, edited by T. Ohsawa and T. Fukahori, JAERI-Conf. 2004–2005 (2004), p. 196.
[25] M. B. Chadwick, P. Oblozinský, M. Herman, N. M. Greene, R. D. McKnight, D. L. Smith, P. G. Young, R. E. MacFarlane, G. M. Hale, S. C. Frankle, A. C. Kahler, T. Kawano, R. C. Little, D. G. Madland, P. Moller, R. D. Mosteller, P. R. Page, P. Talou, H. Trellue, M. C. White, W. B. Wilson, R. Arcilla, C. L. Dunford, S. F. Mughabghab, B. Pritychenko, D. Rochman, A. A. Sonzogni, C. R. Lubitz, T. H. Trumbull, J. P. Weinman, D. A. Brown, D. E. Cullen, D. P. Heinrichs, D. P. McNabb, H. Derrien, M. E. Dunn, N. M. Larson, L. C. Leal, A. D. Carlson, R. C. Block, J. B. Briggs, E. T. Cheng, H. C. Huria, M. L. Zerkle, K. S. Kozier, A. Courcelle, V. Pronyaev, and S. C. van der Marck, Nucl. Data Sheets **107**, 2931 (2006).
[26] G. Rudstam and E. Lund, Nucl. Sci. Eng. **64**, 749 (1977).
[27] G. Rudstam, J. Radioanal. Chem. **36**, 591 (1977).
[28] G. Rudstam, Nucl. Sci. Eng. **80**, 238 (1982).
[29] P. L. Reeder and R. A. Warner, Nucl. Sci. Eng. **79**, 56 (1981).
[30] R.B. Firestone, *Table of Isotopes*, 8th ed. (Wiley & Sons, New York, 1998).
[31] University of Mainz, Institute für Kernphysik 1978 Annual Report.
[32] R. C. Greenwood and A. J. Caffrey, Nucl. Sci. Eng. **91**, 305 (1985).